Synthesis, crystal structure and transport properties of the cluster compounds Tl2Mo15S19 and Ag3Tl2Mo15S19

Patrick Gougeon, Philippe Gall, Shantanu Misra, Anne Dauscher, Christophe Candolfi, Bertrand Lenoir

▶ **To cite this version:**

Patrick Gougeon, Philippe Gall, Shantanu Misra, Anne Dauscher, Christophe Candolfi, et al.. Synthesis, crystal structure and transport properties of the cluster compounds Tl2Mo15S19 and Ag3Tl2Mo15S19. Materials Research Bulletin, 2021, 136, pp.111152. 10.1016/j.materresbull.2020.111152 . hal-03103506

HAL Id: hal-03103506
https://hal.science/hal-03103506

Submitted on 18 Feb 2021

HAL is a multi-disciplinary open access archive for the deposit and dissemination of scientific research documents, whether they are published or not. The documents may come from teaching and research institutions in France or abroad, or from public or private research centers.

L'archive ouverte pluridisciplinaire **HAL**, est destinée au dépôt et à la diffusion de documents scientifiques de niveau recherche, publiés ou non, émanant des établissements d'enseignement et de recherche français ou étrangers, des laboratoires publics ou privés.

Journal Pre-proof

Synthesis, Crystal Structure and Transport Properties of the Cluster Compounds $Tl_2Mo_{15}S_{19}$ and $Ag_3Tl_2Mo_{15}S_{19}$

Patrick Gougeon[1,*], Philippe Gall[1], Shantanu Misra[2], Anne Dauscher[2], Christophe Candolfi[2], Bertrand Lenoir[2]

[1] *Sciences Chimiques de Rennes, UMR 6226 CNRS – INSA - Université de Rennes 1, Avenue du Général Leclerc, 35042 Rennes, France*

[2] *Institut Jean Lamour, UMR 7198 CNRS – Université de Lorraine, 2 allée André Guinier-Campus ARTEM, BP 50840, 54011 Nancy Cedex, France*

[*]Corresponding author: patrick.gougeon@univ-rennes1.fr

Graphical abstract

Journal Pre-proof

Journal Pre-proof

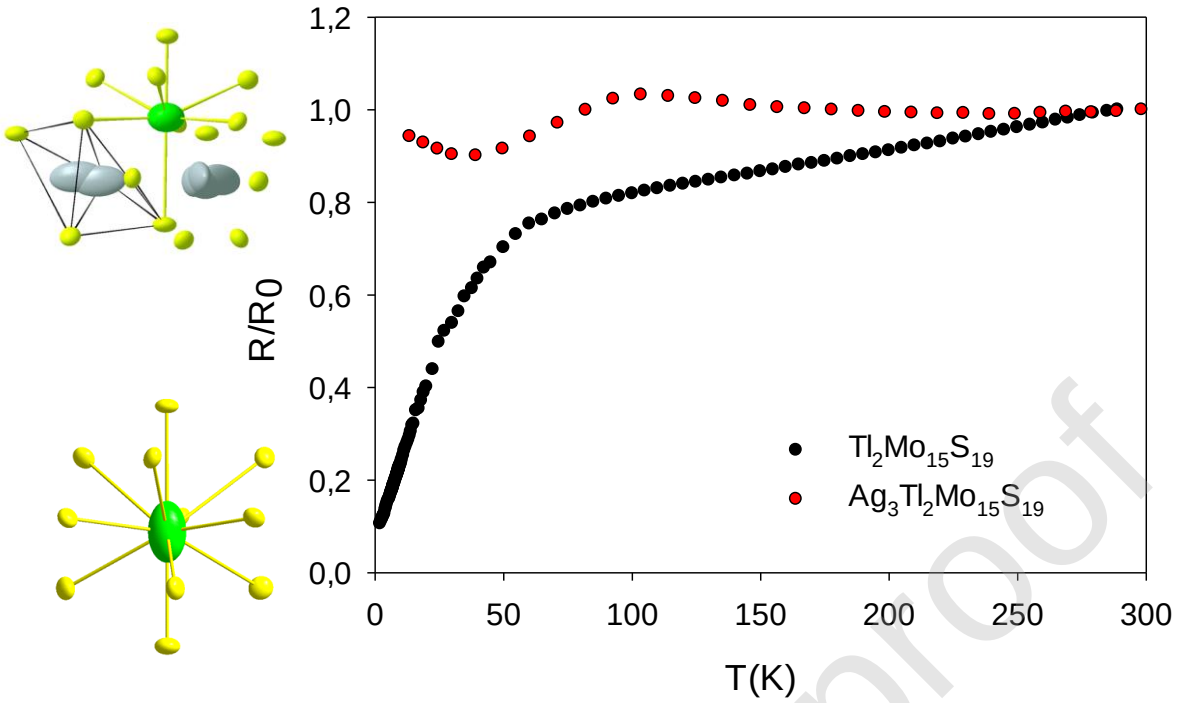

Highlights

- Successful synthesis of single-crystals of $Tl_2Mo_{15}S_{19}$
- Successful synthesis of polycrystalline $Ag_3Tl_2Mo_{15}S_{19}$
- Both crystal structures contain octahedral and bioctahedral clusters in equal proportion
- $Tl_2Mo_{15}S_{19}$ is a *p*-type metal with low electrical resistivity
- Maximum *ZT* value of 0.20 at 800 K in $Ag_3Tl_2Mo_{15}S_{19}$

Abstract

Journal Pre-proof

Journal Pre-proof

We report the syntheses and crystal structures of the cluster compounds $Tl_2Mo_{15}S_{19}$ and $Ag_3Tl_2Mo_{15}S_{19}$, two novel members of the series $M_2Mo_{15}X_{19}$ (M = In, Tl, K, Rb, Cs, Ba; X = S, Se). While only single crystals of $Tl_2Mo_{15}S_{19}$ were obtained, $Ag_3Tl_2Mo_{15}S_{19}$ powders were synthesized, allowing for a study of its thermoelectric properties. Their structures contain $Mo_6S_8{}^iS_6{}^a$ and $Mo_9S_{11}{}^iS_6{}^a$ units separated by Tl^+ cations. Silver insertion increases the electron transfer towards the Mo clusters leading to modifications of the Mo-Mo distances. Electrical resistivity measurements on $Tl_2Mo_{15}S_{19}$ evidence its metallic character. Inserting Ag drives the transport properties towards a semiconducting state characterized by relatively low electrical resistivity and thermopower values. The large, complex unit cell of these compounds results in very low lattice thermal conductivity values below 1 $Wm^{-1}K^{-1}$. Although the Ag insertion improves the thermoelectric performances, the ZT value remains moderate with a maximum value of 0.2 at 800 K.

Keywords

Reduced molybdenum sulphide, molybdenum clusters, thallium, silver, thermoelectric properties.

Journal Pre-proof

Journal Pre-proof

1. Introduction

The Chevrel phases $M_xMo_6X_8$ (M = Na, K, Ca, Sr, Ba, Sn, Pb, 3*d* transition metals or rare earths; X = S, Se or Te) [1] containing octahedral Mo_6 clusters, have been the subjects of numerous studies due to their outstanding physical properties [2-6]. In the early 1980's, sulfide and selenide compounds containing larger clusters such as Mo_9, which can be viewed as the result of the trans-face-sharing of two Mo_6 groups, were successfully characterized. The condensed cluster Mo_9 was first identified in the ternary phase $In_2Mo_{15}Se_{19}$ [7,8] in which it coexists with octahedral Mo_6 clusters in equal proportion. The Mo_6 and Mo_9 clusters are surrounded by 8 and 11 Se atoms, respectively, to form Mo_6Se_8 and Mo_9Se_{11} units that share a part of Se atoms to create large cavities that are occupied by monovalent In^+ cations. Following these reports, isostructural selenides $M_2Mo_{15}Se_{19}$ were isolated with other ternary elements M such as K [9], Rb [10], Ba [11] and Tl [9] as well as sulfides $M_2Mo_{15}S_{19}$ for M = K [12], Rb [13] and Cs [14]. These $M_2Mo_{15}X_{19}$ phases generally exhibit a metallic behavior, show a superconducting transition at low temperatures, and provide another family of compounds in which superconductivity and a charge density wave (CDW) order coexists [15]. Both the superconducting critical temperature, ranging between 1.5 and 4.2 K [9], and the CDW transition temperature depend on the nature of the element M [15].

In addition to these fundamental properties, these compounds meet several requirements to make them interesting candidates for high-temperature thermoelectric applications in power generation, for which high dimensionless thermoelectric figure of merit $ZT = \alpha^2 T/\rho\kappa$ should be achieved. To this end, adjusting the carrier concentration to optimize the thermopower α and the electrical resistivity ρ values as well as a complex unit cell leading to low thermal conductivity κ are the main properties fulfilled by Mo-based cluster compounds. Indeed, the chemical composition of most of these ternary compounds can be manipulated by

Journal Pre-proof

inserting additional elements, such as Ag or Cu, into the large cavities between the cluster units [16-25]. From an electronic point of view, the additional electrons provided by these cations to the host framework contribute to increasing the metallic electron count closer to its optimum value that results in semiconducting properties. This simple guidance, predicted by electronic band structure calculations [22], agrees well with transport property measurements, indicating that the metallic ground state of the ternary compounds is shifted towards a heavily-doped semiconducting state upon Ag or Cu insertion [16-25] resulting in higher α and lower ρ values. Combined with the complex unit cell characterized by a large number of atoms and large, anisotropic thermal displacement parameters of the cations that contribute to limit the thermal transport, these favorable electronic properties yield interesting thermoelectric properties with ZT values reaching 0.45 at $T = 1100$ K in $Ag_3In_2Mo_{15}Se_{19}$ [10,16-27].

While these previous investigations have focused on the Se-based compounds, little is known on the transport properties of their sulfur analogues. In particular, the existence of the selenides $Tl_2Mo_{15}Se_{19}$ and $Ag_3Tl_2Mo_{15}Se_{19}$ [21] naturally raises the question as to whether their sulfide analogues exist. Here, we report the successful synthesis of two novel members of the series of compounds $M_2Mo_{15}X_{19}$, that is, the ternary compound $Tl_2Mo_{15}S_{19}$ and its Ag-filled variant $Ag_3Tl_2Mo_{15}S_{19}$. Although $Tl_2Mo_{15}S_{19}$ could be only prepared in single-crystalline form, a polycrystalline sample of $Ag_3Tl_2Mo_{15}S_{19}$ was successfully synthesized, allowing for a detailed characterization of its transport properties over a broad temperature range (5 – 800 K) and a systematic comparison with its Se counterpart.

Journal Pre-proof

2. Experimental details

2.1 Synthesis and Crystal Growth

All handlings of elements and precursors were performed in a dry, argon-filled glove box. The compounds were synthesized from stoichiometric mixtures of MoS_2, Tl_2S, Mo powders and Ag shots. The Mo powder was first reduced under a stream of H_2 at 1000°C for ten hours to remove traces of oxygen. The precursors MoS_2 and Tl_2S were synthesized by heating the elements Mo, Tl, and S in stoichiometric ratios in silica tubes sealed under a vacuum of about 10^{-2} mbar during 2 days at 800 and 500 °C, respectively. The initial powder mixture was pressed and placed in a Mo crucible, which was sealed with an arc welding. For the synthesis of $Tl_2Mo_{15}S_{19}$, the crucibles were heated at temperatures between 1200 and 1500°C with a heating rate of 300°C h^{-1}. The different temperatures were maintained for 48 h and then decreased at a rate of 100°C h^{-1} to 1100°C, the temperature at which the furnace was allowed to cool down in "free fall". The various tests intended to synthesize monophasic polycrystalline samples of $Tl_2Mo_{15}S_{19}$ were unsuccessful and only resulted in mixtures of phases. While the $Tl_2Mo_9S_{11}$ and Mo_2S_3 phases were predominant in syntheses realized below 1350°C, mixtures of $Tl_2Mo_{15}S_{19}$ and $Tl_2Mo_9S_{11}$ were obtained above this temperature. However, $Tl_2Mo_{15}S_{19}$ single crystals grew during these different attempts and could be isolated, which allowed us to determine the crystal structure of this compound.

In the case of $Ag_3Tl_2Mo_{15}S_{19}$, monophasic polycrystalline samples (Figure 1) could be obtained by heating the starting reagents at 1300°C for 48 h in sealed molybdenum crucibles. Single crystals were obtained by a rapid rise in temperature at 1700°C (heating rate of 600°C

Journal Pre-proof

h^{-1}), followed by a dwell at this temperature for 10 min and by a cooling to 1100°C at 100°C h^{-1}.

2.2 Hot Uniaxial Pressing (HUP)

The polycrystalline $Ag_3Tl_2Mo_{15}S_{19}$ pellet was ground into fine powders and subsequently densified by HUP sintering under a vacuum of about 10^{-2} mbar in order to measure its thermoelectric properties. Approximately 5g of powders were introduced into a graphite die of 10 mm in diameter previously covered with a thin boron nitride layer. The applied pressure was 50 MPa at the start of the heating ramp and was slowly increased to 85 MPa at the sintering temperature of 1300°C, which was held for 2 h. The density of the pellet, determined from its geometrical dimensions and weight, was about 98% of the theoretical density calculated from the crystallographic data.

2.3 Single Crystal Structure Determination

The X-ray diffraction data were collected at 300 K either on a Nonius CAD-4 diffractometer in the case of $Tl_2Mo_{15}S_{19}$ or on an Enraf-Nonius Kappa CCD goniometer for $Ag_3Tl_2Mo_{15}S_{19}$. In both cases, the MoKα radiation (λ = 0.71073 Å) was used. The absorption corrections were applied using the φ-scan method [28] in the case of $Tl_2Mo_{15}S_{19}$ or, for $Ag_3Tl_2Mo_{15}S_{19}$, after determination of the crystal shape, by using an analytical absorption correction developed by de Meulenaer and Tompa [29]. The crystal structures were solved by isomorphism with $In_2Mo_{15}Se_{19}$ and $Ag_3In_2Mo_{15}Se_{19}$. All structure refinements and Fourier analyses were carried out using JANA2006 [29]. The initial models were refined anisotropically down to $R = 0.0471$. At this stage, a difference-Fourier map showed significant electron densities near the Tl atoms (10.23/-10.38 e $Å^{-3}$). A similar situation was

Journal Pre-proof

also observed for the Tl atoms in the Ag-filled compound $Ag_3Tl_2Mo_{15}Se_{19}$ [21]. A three and five-order tensor in the Gram-Charlier expansion [30] of the Tl displacement factor was used to better describe the electronic density around the cationic site in $Ag_3Tl_2Mo_{15}S_{19}$ and $Tl_2Mo_{15}S_{19}$, respectively. The residual peaks near the Tl atom dropped to 2.38 and -1.49 $e^-Å^{-3}$ in the case of $Tl_2Mo_{15}S_{19}$ and 1.46 and -1.15 $e^-Å^{-3}$ for $Ag_3Tl_2Mo_{15}S_{19}$. The non-harmonic probability density function maps of Tl did not reveal significant negative region, confirming the validity of our models [31]. Figure 2 illustrates the non-harmonic probability density isosurface for Tl in $Tl_2Mo_{15}S_{19}$. Refinement of the occupancy factor of the Tl position indicated a full occupation in both compounds. On the other hand, a slight silver deficiency was found for the single crystal investigated with a final stoichiometry corresponding to $Ag_{2.92(2)}Tl_2Mo_{15}S_{19}$. Experimental data and X-ray structural refinement results for the $Tl_2Mo_{15}S_{19}$ and $Ag_3Tl_2Mo_{15}S_{19}$ compounds are summarized in Table 1. The final fractional atomic coordinates and the equivalent isotropic displacement parameters are given in Table S1, while the main interatomic bond lengths are listed in Table 2.

2.4 Scanning electron microscopy (SEM)

SEM experiments were carried out to further assess the phase purity of the polycrystalline sample of $Ag_3Tl_2Mo_{15}Se_{19}$. Images were collected on a polished surface of a bulk piece of the consolidated pellet in backscattered electron mode (BSE) using a Quanta 650 FEG (FEI). Electron dispersive X-ray spectra were collected to obtain an estimate of the chemical composition at various, randomly-chosen areas.

2.5 Transport properties measurements

Journal Pre-proof

For $Ag_3Tl_2Mo_{15}Se_{19}$, the consolidated cylindrical pellet was cut with a diamond-wire saw into bar- and disc-shaped samples. Electrical resistivity, thermopower and thermal conductivity were simultaneously measured between 5 and 300 K on a bar-shaped sample of dimensions ~2×2×8 mm^3 using the thermal transport option of a physical property measurement system (PPMS, Quantum Design). Four copper leads were attached onto the samples using a small amount of conductive silver epoxy. Hall effect measurements were carried out using the ac transport option of the PPMS. The electrical contacts were realized in a five-probe configuration using five copper wires attached with a minute amount of conducting silver paint. The transverse electrical resistivity ρ_{xy} was measured at 300 K under magnetic fields $\mu_0 H$ ranging between – 1T and + 1T. The Hall resistivity ρ_H was then calculated using the formula $\rho_H = \left[\rho_{xy}(+\mu_0 H) - \rho_{xy}(-\mu_0 H)\right]/2$ to dismiss a possible additional magnetoresistive contribution. The Hall coefficient R_H was inferred from the slope of $\rho_H(\mu_0 H)$ in the limit $\mu_0 H \to 0$.

Electrical resistivity and thermopower were measured between 300 and 800 K on a bar-shaped sample using a ZEM-3 apparatus (Ulvac-Riko) under a low helium pressure. Thermal diffusivity measurements were performed in the same temperature range on a disc-shaped sample of 10 mm in diameter using a laser flash instrument (LFA 427, Netzsch). The thermal diffusivity a is related to the thermal conductivity via the relation $\kappa = aC_p\alpha_V$ where C_p is the specific heat and α_V is the experimental density. While C_p was approximated by the Dulong-Petit value ($C_p = 3NR$ where N is the number of atoms per formula unit and R is the gas constant), the temperature dependence of α_V has not been considered in the present case. An overall good match around 300 K between the low-temperature and high-temperature data sets was observed, except for the κ values of the $Ag_3Tl_2Mo_{15}S_{19}$ sample, for which a larger mismatch is observed. This discrepancy is due to thermal radiations that inevitably

Journal Pre-proof

accompany the low-temperature measurements and result in an artificial increase in the measured κ values upon approaching room temperature.

The temperature dependence of the electrical resistivity of $Tl_2Mo_{15}S_{19}$ was determined by measurements on a single crystal using a conventional ac four-probe method with a current of 0.1 mA. Contacts on the single crystal were ultrasonically made with molten indium. The ohmic behaviour and invariance of the phase were checked during the different measurements at low and room temperatures.

3. Results and Discussion

3.1 Crystalline Structures and Phase Purity

The $Tl_2Mo_{15}S_{19}$ compound is isomorphous to the structural type $In_2Mo_{15}Se_{19}$ described for the first time in 1981 [8]. Consequently, its crystalline structure is based on $Mo_6S^i_8S^a_6$ and $Mo_9S^i_{11}S^a_6$ units (Figure 3; for explanations on the *i*- and *a*-type notation, see reference [32]) in equal proportion that share some of their sulfur atoms to form the tridimensional Mo-S framework (Figure 4). The $Mo_6S^i_8S^a_6$ unit is similar to that encountered in the well-known Chevrel-Sergent phases and consist of an Mo_6 octahedral cluster, the eight faces of which are capped by S^i atoms that form a distorted S^i_8 cube and six additional S^a atoms in apical position with respect to the Mo_6 octahedron. The second unit, $Mo_9S^i_{11}S^a_6$, is based on a bioctahedral Mo_9 core resulting from the condensation of two octahedral Mo_6 clusters. The Mo_9 cluster has an environment of 11 face-capping S^i atoms and 6 S^a atoms above the terminal Mo2 atoms. The centers of the $Mo_6S^i_8S^a_6$ and $Mo_9S^i_{11}S^a_6$ units correspond to the 6*a* and 6*b* Wyckoff positions. Consequently, the respective symmetries of the $Mo_6S^i_8S^a_6$ and $Mo_9S^i_{11}S^a_6$ units are $\overline{3}$ and 32. Within the Mo_6 cluster, the Mo-Mo bond lengths are 2.6786(9) Å for the bonds

Journal Pre-proof

between the Mo1 atoms generated by the 3-fold axis, and thus forming a $(Mo1)_3$ triangle perpendicular to the 3-fold axis (also called intra-triangle Mo-Mo bonds), and 2.7727(9) Å for the bonds between Mo1 atoms of adjacent triangles $(Mo1)_3$ (inter-triangle Mo-Mo bonds). In the bioctahedral Mo_9 aggregate, the Mo-Mo bond lengths are 2.6812(9) and 2.6865(7) Å for the intra-triangle Mo2-Mo2 and Mo3-Mo3 bonds distances, respectively, and the two inter-triangle distances between the $(Mo2)_3$ and $(Mo3)_3$ triangles are 2.7103(8) and 2.7844(8) Å. While the S1, S2, S4 and S5 atoms only cap one triangular face of the Mo_6 or Mo_9 clusters, the median S3 atom in the Mo_9 cluster caps two faces. In addition, the S1 and S2 atoms are bonded to a Mo2 or Mo1 atom of an adjacent Mo_9 or Mo_6 cluster, respectively. The Mo-S bond lengths are comprised between 2.4234(14) and 2.4708(13) Å in the $Mo_6S^i_8S^a_6$ entity and between 2.3933(14) and 2.6167(10) Å in the $Mo_9S^i_{11}S^a_6$ cluster. The shortest intercluster Mo1-Mo2 distance between the Mo_6 and Mo_9 clusters is 3.1983(9) Å, suggesting very weak direct interactions between both clusters. The Tl^+ cations are localized in large cavities formed by five $Mo_6S^i_8S^a_6$ and three $Mo_9S^i_{11}S^a_6$ units. Their environment consists of 11 S atoms forming a penta-capped trigonal prism (Figure 5a). This Tl environment corresponds to the Edshammar 11-polyhedron presents in the Ni_2In type structures [33]. The Tl-S bond lengths are between 3.1523(13) and 3.7118(14) Å. The average Tl-S distance is 3.50 Å, which is close to 3.54 Å, a value corresponding to that expected from the sum of the radii of the anion S^{2-} and cation Tl^+ in 12-coordination environment reported by Shannon [34]. The bond-valence sums (BVS) of the Tl atom was calculated with BV coefficients as given by Brown and Altermatt [35]. Sulphur atoms within a maximal distance of 4.5 Å of the Tl atom were included in the calculation. The calculated BVS of the Tl atoms is +1.051(2), that is, close to the ideal value of +1.

In the $Ag_3Tl_2Mo_{15}S_{19}$ compound, the Ag atoms occupy distorted trigonal bipyramidal sites of S atoms located between two consecutive Tl sites (Figure 5b). However, due to the

Journal Pre-proof

proximity of the Ag sites that are delocalized on either side of the triangular base and only distant of 0.9 Å, the Ag atoms are found in pseudo-tetrahedral sites of sulfur atoms. The insertion of Ag modifies drastically the Tl environment since the latter moves towards the S5 atom and moves away from the sulfur atoms S3 and S4. As a result, the Tl atoms exhibit an environment composed of seven S atoms with four of them, three S2 and one S5, forming an irregular tetrahedron, while the other three (S1) bridge the three faces of the tetrahedron (see Figure 5b). In $Ag_3Tl_2Mo_{15}S_{19}$, the BVS calculated are +1.06(2) for Ag and 1.11(2) for Tl. Our attempts to calculate the BVS for the Mo atoms by using different coefficients published in references 35 and 36 were unsuccessful, probably due to the influence of strong metal–metal bonding.

The different Mo-Mo bond lengths in the two Mo aggregates are shown in Figure 6 for $Ag_3Tl_2Mo_{15}S_{19}$, $Tl_2Mo_{15}S_{19}$, $K_2Mo_{15}S_{19}$, $Rb_2Mo_{15}S_{19}$ and $Cs_2Mo_{15}S_{19}$, which are the only sulfur-based compounds crystallizing in the $In_2Mo_{15}Se_{19}$ structure type. As can be seen, the size of the cation has only little influence. The largest differences between the K and Cs compounds concern the inter-triangle bonds Mo1-Mo1 and Mo2-Mo3 in the Mo_6 and Mo_9 aggregates that decrease by 0.01 Å and increase by 0.017 Å, respectively. On the other hand, the Mo-Mo bonds in the quaternary compounds (represented by squares in Figure 6) did not follow the trends of the other compounds. Indeed, as previously observed for the selenides $In_2Mo_{15}Se_{19}$ and $Tl_2Mo_{15}Se_{19}$, Ag insertion modifies the Mo-Mo bond lengths in the Mo_6 and Mo_9 aggregates. Thus, when the cationic charge increases from +2 in $Tl_2Mo_{15}S_{19}$ to +5 in $Ag_3Tl_2Mo_{15}S_{19}$, assuming that both Tl and Ag possesses an oxidation state of +1, the intra-triangle distances Mo1-Mo1 in the octahedral Mo_6 cluster (distances between Mo1 atoms related through the threefold axis) remain almost identical in the ternary and quaternary compounds. In contrast, a decrease of 0.066 Å in the inter-triangle distances Mo1-Mo1 is observed due to its bonding character. In the Mo_9 cluster, an increase (0.034 Å) in the intra-

Journal Pre-proof

triangle distances Mo3-Mo3 is observed since the latter bond is antibonding. The other distances in the Mo_9 cluster, intra-triangle Mo2-Mo2 and inter-triangle Mo2-Mo3, decreases as the cationic charge increases, reflecting their bonding character. Regarding the unit-cell parameters, the presence of Ag results in an increase in the *a* parameter, which mainly comes from a sterical effect. On the other hand, the decrease in the *c* parameter can be attributed to a shortening of the clusters along this axis, resulting from the shortening of the inter-triangle Mo-Mo bond lengths in the Mo_6 and Mo_9 clusters and the electronic effect related to the increase in the number of electrons on both clusters as mentioned above.

The phase purity of the polycrystalline sample of $Ag_3Tl_2Mo_{15}S_{19}$ has been further verified by SEM images (Figure 7) collected in backscattered electron mode (BSE). These experiments reveal the presence of minute amount of a secondary phase, determined to be X, in addition to the main $Ag_3Tl_2Mo_{15}S_{19}$ phase. The chemical composition, estimated by energy-dispersive electron microscopy (EDS) to be $Ag_{2.67}Tl_{2.69}Mo_{15}S_{18.96}$ (normalized to 15 Mo atoms per chemical formula), is close to the nominal composition. We note that this chemical composition should be taken with some caution due to the strong overlap of the main emission lines of Ag, Mo and S. Nevertheless, EDX spectra taken at randomly-chosen spots did not indicate significant variations in these contents, suggesting the absence of significant spatial fluctuations, notably in the Ag and Tl contents. Fracture image (Fig. 7b), representative of the polycrystalline sample of $Ag_3Tl_2Mo_{15}S_{19}$, shows a microstructure similar to that observed in other Ag-filled cluster compounds such as $Ag_3K_2Mo_{15}Se_{19}$.[24] Despite the strongly-elongated crystal structure of these compounds, no clear tendency of preferential alignment of the crystallite is observed, in agreement with the PXRD pattern.

3.2 Transport properties

Journal Pre-proof

Assuming a +1 valence state of the Tl atoms, the metallic electron count (MEC) of $Tl_2Mo_{15}S_{19}$ is predicted to be equal to 54, which is significantly lower than the optimum MEC of 60 required to reach a semiconducting state [22]. In agreement with these considerations, $Tl_2Mo_{15}S_{19}$ exhibits a metallic behavior over the entire temperature range (Figure 8a), with no evidence for a superconducting transition down to 1.8 K.

Despite an expected increase in the MEC to 57 upon inserting Ag, a metallic-like behavior is still observed in the $Ag_3Tl_2Mo_{15}S_{19}$ compound, with electrical resistivity ρ values hardly evolving upon cooling from 16 μΩ.m at 800 K to 15 μΩ.m near 100 K (Figure 8b). At this temperature, ρ shows a maximum before decreasing upon further cooling to 35 K where a minimum is reached. Further lowering the temperature then results in a slight increase in ρ. While ρ varies in a similar manner in the S and Se compounds between 150 and 800 K, this low-temperature non-monotonic behavior in the former contrasts with the monotonic increase in ρ observed in the latter. This complex evolution with temperature might reflect a multiband character of the transport in $Ag_3Tl_2Mo_{15}S_{19}$. The fact that similar properties are observed in the S and Se compounds is coherent with results reported on the Chevrel phases [1-3] for which, substituting S for Se does not alter the metallic character of the compound. However, both elements are not strictly equivalent and suggest that both compounds exhibit different carrier concentrations and mobilities. Measurements of the room-temperature Hall coefficient in $Ag_3Tl_2Mo_{15}S_{19}$ tends to support this hypothesis with a measured value on the order of 10^{-3} $cm^3\ C^{-1}$. The order of magnitude of this value is equivalent to those measured below 150 K in $Ag_3Tl_2Mo_{15}Se_{19}$ [21]. Of note, Hall measurements in these compounds is difficult due to their degenerate nature and the presence of hole and electron contributions that result in nearly-null, strongly noisy signals. It is thus likely that replacing Se by S tips the balance between both contributions resulting in differences in the temperature dependence and values of the Hall coefficient.

Journal Pre-proof

The temperature dependence of the thermopower α, shown in Figure 8c, provides another experimental evidence that both S and Se are not electronically equivalent in these compounds. The positive α values characterizing both compounds, indicative of holes as the dominant charge carrier, are lower in the S compound compared to the Se analogue over the entire temperature range. For both compounds, α monotonically increases with increasing temperature to reach 75 and 65 μV K^{-1} at 800 K in the Se and S compounds, respectively. In neither case is $\alpha(T)$ linear as it would be expected for a purely diffusive regime in a metallic system. In contrast, $Ag_3Tl_2Mo_{15}S_{19}$ features a non-linear evolution below 200 K marked by a broad maximum near 100 K, that is, in the temperature region where the upturn in ρ is observed. In addition to the multiband character of the transport suggested by these temperature dependences, the presence of holes and electrons contributing to the transport may be another ingredient explaining the differences observed between the S and Se analogues. The presence of both charge carriers has been systematically observed in compounds formed by $Mo_{15}Se_{19}$ clusters [16,21,24], regardless of the nature of the filling cations. As for the Hall coefficient, the substitution of S for Se might tip the balance between the contributions of both carriers, eventually altering the measured α values.

Figure 9a shows the total thermal conductivity κ as a function of temperature for $Ag_3Tl_2Mo_{15}S_{19}$ and $Ag_3Tl_2Mo_{15}Se_{19}$. The overall behavior of $\kappa(T)$ is consistent with the glass-like temperature dependence observed ubiquitously in Mo-based cluster compounds [10,16-27], regardless of the nature of the cations and of the size and geometry of the cluster units. For both compounds, κ increases with increasing temperature to reach 1.5 and 1.3 W m^{-1} K^{-1} at 750 K in the S and Se compounds, respectively. The main differences are related to the higher κ values in the S compound and the small but visible change of slope near 80 K, absent in the Se analogue. This temperature corresponds to the maximum observed in $\alpha(T)$ and, most notably, to the upturn observed in $\rho(T)$. The fact that this anomaly is consistently

Journal Pre-proof

observed in all transport properties further supports the presence of a possible structural or electronic phase transition.

The electronic contribution to the thermal conductivity, κ_e, was determined using the Wiedemann-Franz law $\kappa_e = LT/\rho$ where L is the Lorenz number. Due to the highly-degenerate nature of the transport in both compounds, L was assumed to be equal to the value of a degenerate hole gas $L_0 = 2.44\times10^{-8}$ V^2 K^{-2} below 300 K. Above room-temperature, the temperature dependence of L was approximated by a single-parabolic band model. The temperature dependence of the lattice thermal conductivity $\kappa_{ph} = \kappa - \kappa_e$, shown in Figure 9b, evidences very low values on the order of 0.7 W m^{-1} K^{-1}, that are practically temperature independent above room temperature. The κ_{ph} values are slightly higher than those characterizing the Se analogue [21], suggesting that the thermal transport does not significantly depend on the nature of the chalcogen atoms forming the Mo clusters. For $Ag_3Tl_2Mo_{15}Se_{19}$, κ_{ph} approaches the minimum lattice thermal conductivity $\kappa_{min} \approx 0.38$ W m^{-1} K^{-1} estimated using the model developed by Cahill and Pohl [37]

$$\kappa_{min} = \frac{1}{2}\left(\frac{\pi}{6}\right)^{-1/3} k_B V^{-2/3}(2v_T + v_L) \qquad (1)$$

where V is the average volume per atom, v_T and v_L are the transverse and longitudinal sound velocity, respectively. v_T and v_L were measured at 300 K using a pulse-echo method and found to be equal to 1680 and 3350 m s^{-1}, respectively. In contrast, the κ_{ph} values of the S analogue remains slightly higher, reaching 0.5 W m^{-1} K^{-1} at 765 K. This difference between both compounds may be explained by the different density of the S and Se compounds, which contributes to the higher κ_{ph} values observed in the former. A decrease in the density will

Journal Pre-proof

tend to increase the transverse and longitudinal sound velocities, depending on the variations in the stiffness when replacing Se by S.

The overall poor ability of $Ag_3Tl_2Mo_{15}S_{19}$ to transport heat mainly results from the presence of both Ag and Tl, the positional and dynamic disorder of which gives rise to low-energy optical modes that contribute to strongly limit the dispersion of acoustic phonons. This important trait of Mo-based cluster compounds has notably been experimentally evidenced by inelastic X-ray scattering in the quasi-one dimensional series $A_2Mo_6Se_6$ (*A* = K, Rb, Cs, In and Tl) for which the low-energy lattice dynamics is dominated by modes associated with the thermal motion of the *A* cations [38]. These measurements have also established the absence of significant anharmonicity or avoided-crossing dispersions that would be expected in a rattling-like scenario. Whether these conclusions can be extended to the present family of compounds will require similar investigations of their lattice dynamics.

The combination of the three transport coefficients yields the temperature dependence of the dimensionless thermoelectric figure of merit *ZT* (Figure 9c). A maximum *ZT* value of 0.15 is achieved at 800 K in $Ag_3Tl_2Mo_{15}S_{19}$, which is comparable to the peak value of 0.18 at 750 K obtained in the Se analogue $Ag_3Tl_2Mo_{15}Se_{19}$ [21]. This moderate value is mainly due to the rather low thermopower values measured at high temperatures, suggesting that the carrier concentration remains too high to reach higher thermoelectric performances. The nature of the chalcogen atoms forming the cluster units seems to be of minor influence in determining the thermoelectric performances in this family of compounds. Because the highest *ZT* value has been achieved so far in the In-filled compound $Ag_3In_2Mo_{15}Se_{19}$ (0.25 at 800 K), it would be interesting to determine whether similar thermoelectric properties are observed in the hypothetical sulfur compound $Ag_3In_2Mo_{15}S_{19}$.

4. Summary and Conclusion

Journal Pre-proof

Two novel reduced molybdenum sulfides $Tl_2Mo_{15}S_{19}$ and $Ag_3Tl_2Mo_{15}S_{19}$ have been successfully synthesized by solid-state reactions in sealed molybdenum crucibles. As in $In_2Mo_{15}Se_{19}$ [8], their crystal structure contains octahedral Mo_6 and bioctahedral Mo_9 clusters in equal proportion forming $Mo_6S^i_8S^a_6$ and $Mo_9S^i_{11}S^a_6$ cluster units with S atoms. These two units are separated from each other by large voids that are filled up by eleven-coordinated Tl atoms. In agreement with the predicted metallic electron count, $Tl_2Mo_{15}S_{19}$ behaves as a *p*-type metal with relatively low electrical resistivity. Despite an increase in the MEC induced by the insertion of Ag, the Ag-filled compound shows metallic-like transport with moderate thermopower values. Changing the nature of the chalcogen atoms from Se to S does not significantly alter the key characteristics of the thermal transport observed in these cluster compounds, that is, a glass-like temperature dependence that accompanies very low lattice thermal conductivity values. The metallic character of $Ag_3Tl_2Mo_{15}S_{19}$ leads to a moderate peak *ZT* value of 0.15 at 800 K, similar to that achieved in the Se analogue $Ag_3Tl_2Mo_{15}Se_{19}$. Further investigations with other cations will be interesting to determine whether improved thermoelectric performances can be achieved in this broad family of compounds.

Acknowledgements

The authors thank the financial support of the French Agence Nationale de la Recherche (ANR), through the program Energy Challenge for Secure, Clean and Efficient Energy (Challenge 2, 2015, ANR-15-CE05-0027).

Journal Pre-proof

Journal Pre-proof

Author statement_CC

Patrick Gougeon: Structural studies, crystal growth.

Philippe Gall: Powder syntheses.

Shantanu Misra: High-temperature thermal diffusivity measurements

Anne Dauscher: Low-temperature transport properties measurements

Christophe Candolfi: High-temperature electrical resistivity and thermopower measurements

Bertrand Lenoir: Low-temperature transport properties measurements

Declaration of interests

The authors declare that they have no known competing financial interests or personal relationships that could have appeared to influence the work reported in this paper.

Journal Pre-proof

Journal Pre-proof

References

[1] R. Chevrel, M. Sergent, J. Prigent, J. Solid State Chem. 3 (1971) 515.

[2] Ø. Fischer, Appl. Phys. 16 (1978) 1.

[3] O. Pena, M. Sergent, Prog. Solid State Chem. 19 (1989) 165.

[4] D. H. Douglass (ed.), in *Superconductivity in d- and f-band Metals* (Plenum Press, New York, 1986).

[5] G. K. Shenoy, B. D. Dunlap, F. Y. Fradin (eds.), *Ternary Superconductors* (North Holland, New York, Amsterdam, Oxford, 1981).

[6] Ø. Fischer and M. B. Maple (eds.), *Topics in Current Physics*, vol. 32/34: Superconductivity in Ternary Compounds, Tomes I and II. (Springer, Berlin, Heidelberg, New York, 1982).

[7] A. Lipka, K. Yvon, Acta Cryst. B36 (1980) 2123.

[8] M. Potel, R. Chevrel, M. Sergent, Acta Cryst. B37 (1981) 1007.

[9] R. Chevrel, M. Potel, M. Sergent, M. Decroux, Ø. Fischer, Mat. Res. Bull. 15 (1980) 867.

[10] G. Daigre, P. Gougeon, P. Gall, R. Gautier, O. Guillou, J.-B. Vaney, C. Candolfi, A. Dauscher, B. Lenoir, J. Solid State Chem. 237 (2016) 1.

[11] P. Gougeon, M. Potel, M. Sergent, Acta Cryst. C45 (1989) 1285.

[12] S. Picard, P. Gougeon, M. Potel, Acta Cryst. E58 (2002) i12.

[13] S. Picard, J.-Y. Saillard, P. Gougeon, H. Noel, M. Potel, J. Solid State Chem. 155 (2000) 417.

[14] S. Picard, D. Salloum, P. Gougeon, M. Potel, Acta Cryst. C60 (2004) i61.

Journal Pre-proof

[15] C. Candolfi, M. Misek, P. Gougeon, R. Al Rahal Al Orabi, P. Gall, R. Gautier, S. Migot, J. Ghanbaja, J. Kastil, P. Levinsky, J. Hejtmanek, A. Dauscher, B. Malaman, B. Lenoir, Phys. Rev. B 101 (2020) 134521.

[16] P. Gougeon, P. Gall, R. Al Rahal Al Orabi, B. Fontaine, R. Gautier, M. Potel, T. Zhou, B. Lenoir, M. Colin, C. Candolfi, A. Dauscher, Chem. Mater. 24 (2012) 2899.

[17] T. Zhou, M. Colin, C. Candolfi, C. Boulanger, A. Dauscher, E. Santava, J. Hejtmanek, P. Baranek, R. Al Rahal Al Orabi, M. Potel, B. Fontaine, P. Gougeon, R. Gautier, B. Lenoir, Chem. Mater. 26 (2014) 4765.

[18] R. Al Rahal Al Orabi, P. Gougeon, P. Gall, B. Fontaine, R. Gautier, M. Colin, C. Candolfi, A. Dauscher, J. Hejtmanek, B. Malaman, B. Lenoir, Inorg. Chem. 53 (2014) 11699.

[19] R. Al Rahal Al Orabi, B. Fontaine, R. Gautier, P. Gougeon, P. Gall, Y. Bouyrie, A. Dauscher, C. Candolfi, B. Lenoir, Inorg. Chem. 55 (2016) 6616.

[20] P. Gougeon, P. Gall, O. Merdrignac-Conanec, L. Aranda, A. Dauscher, C. Candolfi, B. Lenoir, Inorg. Chem. 56 (2017) 9684.

[21] P. Gougeon, P. Gall, R. Al Rahal Al Orabi, B. Boucher, B. Fontaine, A. Dauscher, C. Candolfi, B. Lenoir, Inorg. Chem. 58 (2019) 5533.

[22] R. Al Rahal Al Orabi, B. Boucher, B. Fontaine, P. Gall, C. Candolfi, B. Lenoir, P. Gougeon, J.-F. Halet, R. Gautier, J. Mater. Chem. C 5 (2017) 12097.

[23] P. Masschelein, C. Candolfi, A. Dauscher, C. Gendarme, R. Al Rahal Al Orabi, P. Gougeon, M. Potel, P. Gall, R. Gautier, B. Lenoir, J. Alloys Compnd 739 (2018) 360.

[24] G. Daigre, P. Gougeon, P. Gall, O. Merdrignac-Conanec, R. Al Rahal Al Orabi, R. Gautier, A. Dauscher, C. Candolfi, B. Lenoir, ACS Appl. Ener. Mater. 3 (2020) 2846.

[25] M. Colin, T. Zhou, B. Lenoir, A. Dauscher, R. Al Rahal Al Orabi, P. Gougeon, M. Potel, P. Baranek, C. Semprimoschnig, J. Electron. Mater. 41 (2012) 1360.

Journal Pre-proof

[26] T. Zhou, B. Lenoir, M. Colin, A. Dauscher, R. Al Rahal Al Orabi, P. Gougeon, M. Potel, E. Guilmeau, Appl. Phys. Lett. 98 (2011) 162106.

[27] S. M. Butorin, K. O. Kvashnina, M. Klintenberg, M. Kavcic, M. Zitnik, K. Bucar, P. Gougeon, P. Gall, C. Candolfi, B. Lenoir, ACS Appl. Ener. Mater. 1 (2018) 4032.

[28] A. Altomare, M. C. Burla, M. Camalli, G. L. Cascarano, C. Giacovazzo, A. Guagliardi, A. G. G. Moliterni, G. Polidori, R. Spagna, J. Appl. Cryst. 32 (1999) 115.

[29] J. de Meulenaer, H. Tompa, Acta Crystallogr. 19 (1965) 1014.

[30] V. Petricek, M. Dusek. Jana 2006; Institute of Physics, Academy of Sciences of the Czech Republic: Prague, Czech Republic, 2006.

[31] C. K. Johnson, H. A. Levy. (1974). International Tables for X-ray Crystallography, Ed. J. A. Ibers & W. C. Hamilton, Vol. IV, pp. 311-336. Birmingham: Kynoch Press.

[32] H. Schäfer, H. G. Von Schnering, Angew. Chem. *20* (1964) 833.

[33] L.-E. Edshammar, *'X-Ray Studies on Binary Alloys of Aluminium with Platinum Metals'*, Dissertation, University of Stockholm 1969.

[34] R. D. Shannon, Acta Cryst. A32 (1976) 751.

[35] I.D. Brown and D. Altermatt, Acta Cryst. B41 (1985) 244-247.

[36] N.E. Brese and M. O'Keeffe, Acta Cryst. B47 (1991) 192-197.

[37] D. G. Cahill, S. K. Watson, R. O. Pohl, Phys. Rev. B 46 (1992), 6131-6140.

[38] L. Gannon, L. Boeri, C. A. Howard, P. Gougeon, P. Gall, M. Potel, D. Salloum, A. P. Petrovic, M. Hoesch, Phys. Rev. B 98 (2018) 014104.

Journal Pre-proof

Journal Pre-proof

Tables

Table 1. Single-crystal data collection and structure refinement of $Tl_2Mo_{15}S_{19}$ and $Ag_3Tl_2Mo_{15}S_{19}$ at 293 K.

Empirical formula	$Tl_2Mo_{15}S_{19}$	$Ag_3Tl_2Mo_{15}S_{19}$
Molar mass ($g.mol^{-1}$)	2456.98	2780.6
Symmetry	Trigonal	
Space group	$R\bar{3}c$	
a (Å)	9.3562 (9)	9.6407 (1)
c (Å)	56.206 (9)	55.6492(9)
V ($Å^3$)	4261.0 (11)	4479.26(10)
Z	6	
ρ ($g.cm^{-3}$)	5.74	6.18
Crystal color and habit	black, irregular	
Crystal size (mm^3)	0.09×0.08×0.06	0.142×0.108×0.075
Radiation	Mo Kα	
θ range (°)	2.17 – 39.99	2.55 – 35.00
Absorption coefficient (mm^{-1})	19.05	20.037
Limiting indices	$0\leq h\leq 16$, $0\leq k\leq 16$, $0\leq l\leq 101$	$-15\leq h\leq 15$, $-15\leq k\leq 14$, $-88\leq l\leq 60$
Reflections collected/unique	2947 / 2928	23584 / 2202
R (int)	0.027	0.117
Absorption correction	ψ scan	analytical
Max./min. transmission	0.381 / 0.294	0.2684 /0.1103
Data/restraints/parameters	1851 / 0 / 73	1945 / 0 /76
R indices [$I>2\sigma(I)$]	R1=0.038, *w*R2=0.045	R1=0.034, *w*R2=0.074

Journal Pre-proof

Largest diff. peak and hole ($eÅ^{-3}$)	3.88/ −2.62	1.67/-1.88
Goodness-of-fit on F^2	1.18	1.63

Table 2. Main Interatomic Bond Lengths (in Å) for $Tl_2Mo_{15}S_{19}$ and $Ag_3Tl_2Mo_{15}S_{19}$.

Mo1-Mo1	2.6786(9)	2.6732(5)
Mo1-Mo1	2.7727(9)	2.6973(5)
Mo1-S4	2.4234(14)	2.4631(13)
Mo1-S2	2.4267(11)	2.4966(9)
Mo1-S1	2.4430(13)	2.4543(11)
Mo1-S1	2.4550(15)	2.4615(13)
Mo1-S1	2.4708(13)	2.4948(15)
Mo2-Mo2	2.6812(9)	2.6479(4)
Mo2-Mo3	2.7103(8)	2.6760(3)
Mo2-Mo3	2.7844(8)	2.7543(4)
Mo2—S5	2.4166 (14)	2.4128(13)
Mo2—S2	2.4254 (13)	2.4404(9)
Mo2—S1	2.4823 (11)	2.5472(12)
Mo2—S2	2.4862 (15)	2.5161(11)
Mo2—S3	2.6167 (10)	2.5800(6)
Mo3-Mo3	2.6865(7)	2.7209(5)
Mo3-S2 (×2)	2.3933 (14)	2.4698(11)
Mo3—S3	2.4700 (18)	2.4509(9)
Mo3—S3	2.4703 (17)	2.4509(8)
Tl-S2 (×3)	3.1523(11)	3.2403(11)
Tl-S4	3.291(2)	3.861(2)
Tl-S5	3.620(2)	2.930(2)
Tl-S1 (×3)	3.7118(14)	3.5059(12)

Journal Pre-proof

Journal Pre-proof

Tl-S3 (×3)	3.644(2)	4.0975(8)
Ag-S3		2.4390(14)
Ag-S2		2.6423(17)
Ag-S2		2.6912(16)
Ag-S4		2.8469(13)

Figure Captions

Fig. 1. Profile matching refinement of the powder X-ray diffraction patterns of $Ag_3Tl_2Mo_{15}S_{19}$ (λ = 1.5406 Å). The red circles, black line and bottom blue line correspond to the experimental, calculated and difference profile, respectively. All reflections could be indexed using the crystal structure determined from single-crystal refinements. The vertical ticks mark the calculated positions of the reflections.

Fig. 2. Non-harmonic probability density isosurface of the Tl atoms in $Tl_2Mo_{15}S_{19}$. The S atoms are drawn at an arbitrary size. The level of the three-dimensional maps is at 0.1 $Å^{-3}$.

Fig. 3. View of $Tl_2Mo_{15}S_{19}$ (right) and $Ag_3Tl_2Mo_{15}S_{19}$ (left) projected along the [110] direction. Thermal displacement ellipsoids are drawn at the 97% probability level.

Fig. 4. View showing the atom-numbering scheme and the interunit linkage of the $Mo_9S_{11}S_6$ and $Mo_6S_8S_6$ cluster units. Thermal displacement ellipsoids are drawn at the 97% probability level.

Fig. 5. a) Sulfur environment of the Tl^+ cations in $Tl_2Mo_{15}S_{19}$. **b)** Sulfur environment of the Tl^+ and Ag^+ cations in $Ag_3Tl_2Mo_{15}S_{19}$.

Journal Pre-proof

Fig. 6. Variations in the Mo-Mo bond lengths in the Mo_6 and Mo_9 clusters for the $Ag_3Tl_2Mo_{15}S_{19}$ (filled squares) and $M_2Mo_{15}S_{19}$ (M = Tl, K, Rb, and Cs; filled circles) compounds. Solid lines are guides to the eye.

Fig. 7. a) SEM image in backscattered electron mode (BSE) representative of the good chemical homogeneity of the polycrystalline sample of $Ag_3Tl_2Mo_{15}S_{19}$. b) Typical fracture image obtained on a freshly-broken polycrystalline piece taken from the consolidated pellet. The microstructure is similar to that observed in the $Ag_3K_2Mo_{15}Se_{19}$ compound (Ref. 24).

Fig. 8. Temperature dependence of a) the electrical resistivity ρ of a $Tl_2Mo_{15}S_{19}$ single crystal, b) the electrical resistivity ρ and c) thermopower α of polycrystalline $Ag_3Tl_2Mo_{15}S_{19}$. For comparison purposes, the data measured in the Se analogue $Ag_3Tl_2Mo_{15}Se_{19}$ have been added. The color-coded symbols are similar in panels b and c.

Fig. 9. Temperature dependence of a) the total thermal conductivity κ, b) lattice thermal conductivity κ_{ph} and c) dimensionless thermoelectric figure of merit ZT for $Ag_3Tl_2Mo_{15}S_{19}$. For comparison purposes, the data measured in the Se analogue $Ag_3Tl_2Mo_{15}Se_{19}$ have been added. The color-coded symbols are similar in all the three panels. The horizontal solid line in panel b) stands for the minimum thermal conductivity κ_{min} estimated using the Eq.(1) (Ref. [37]). The mismatch observed near room temperature between the low-temperature and high-temperature data for $Ag_3Tl_2Mo_{15}S_{19}$ in panel a) is due to thermal radiations that yield an extrinsic, additional contribution to the low-temperature data.

Journal Pre-proof

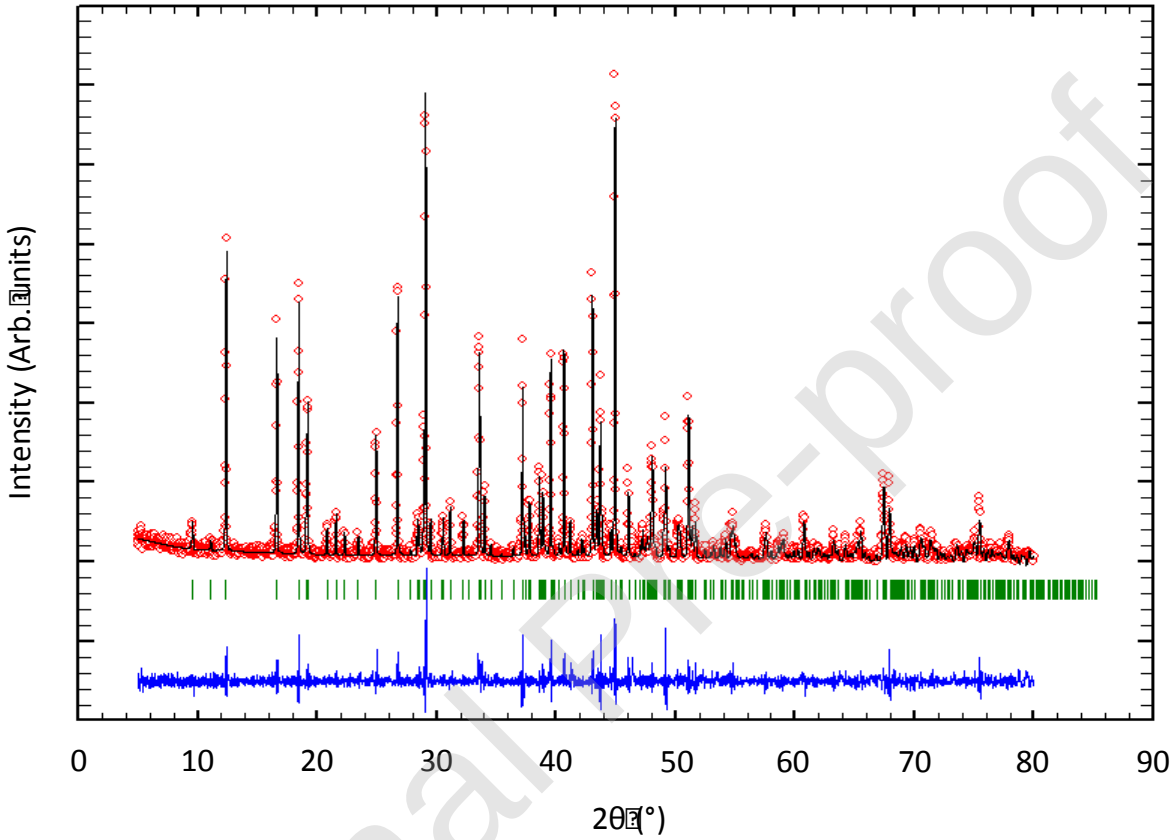

Figure 1

Journal Pre-proof

Journal Pre-proof

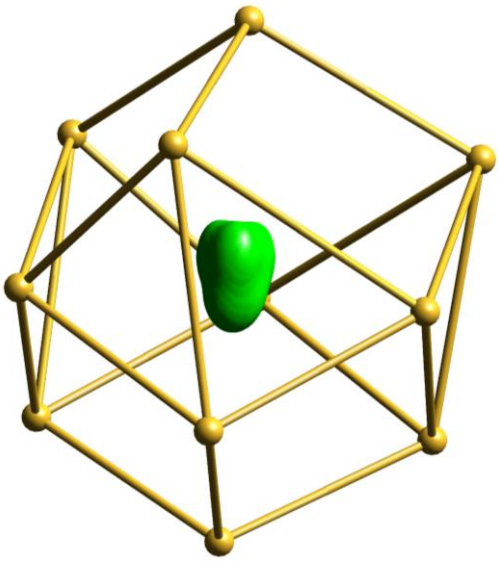

Figure 2

Journal Pre-proof

Journal Pre-proof

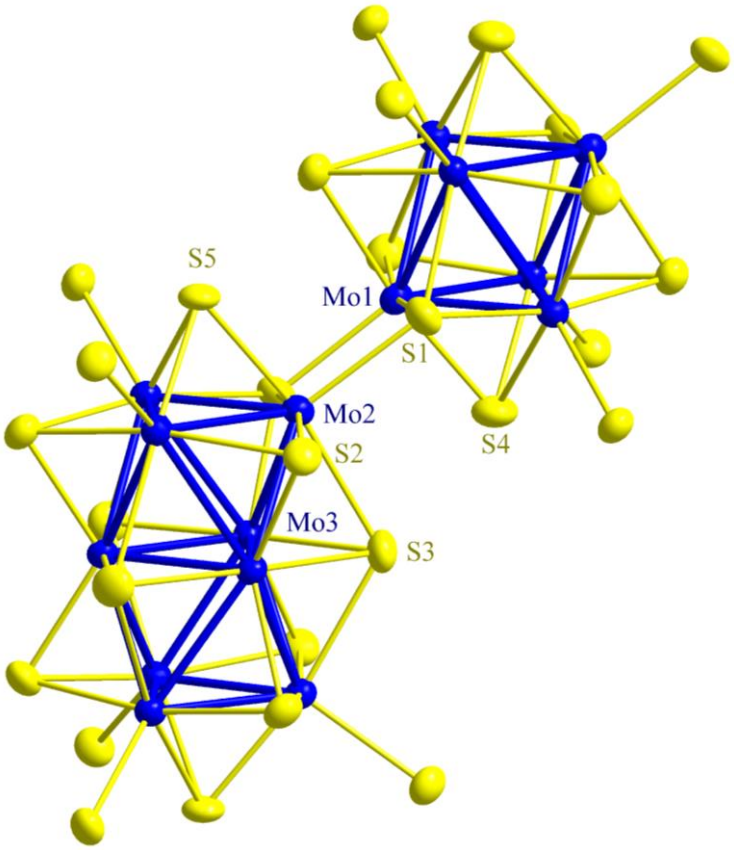

Figure 3

Journal Pre-proof

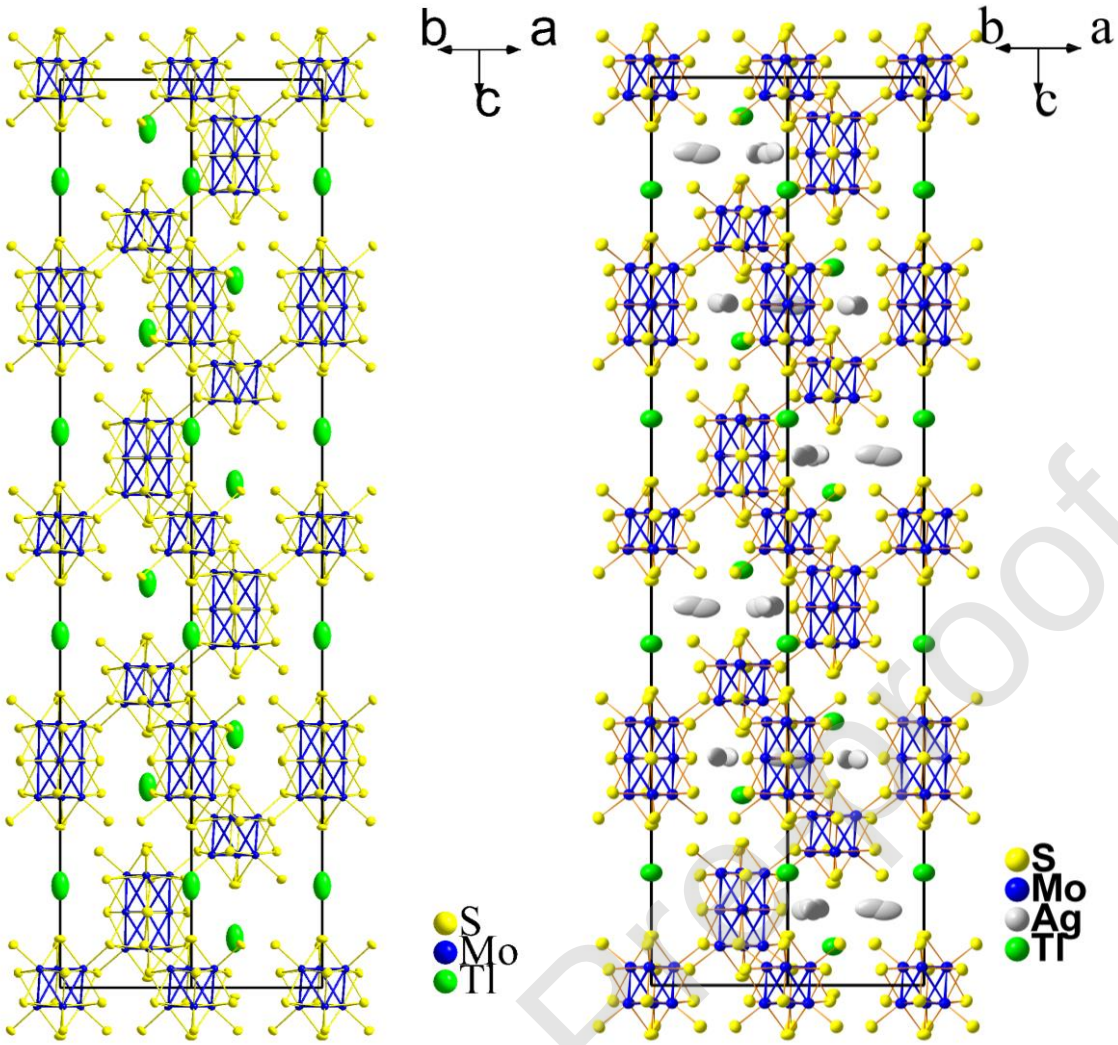

Figure 4

Journal Pre-proof

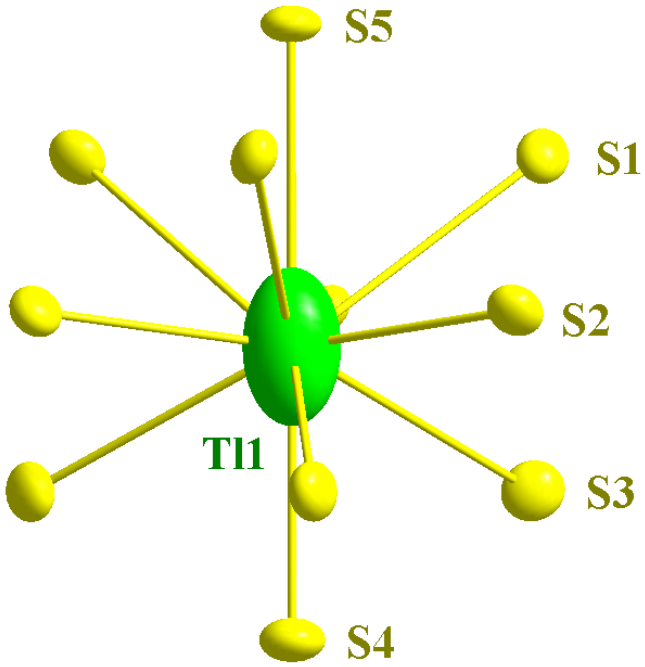

a)

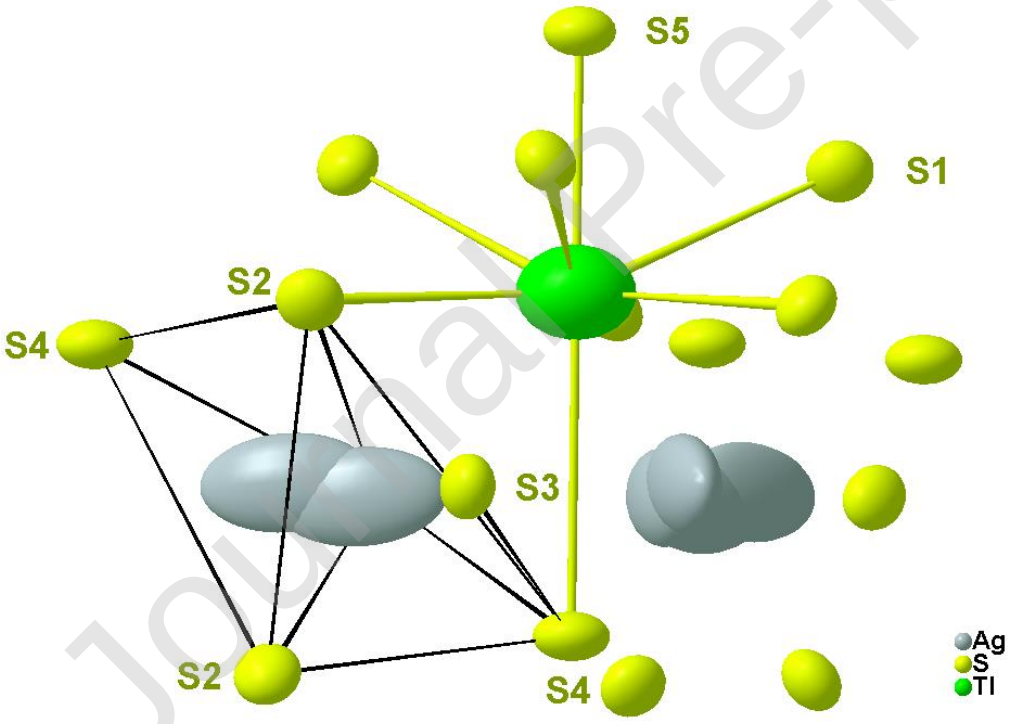

b)

Figure 5

Journal Pre-proof

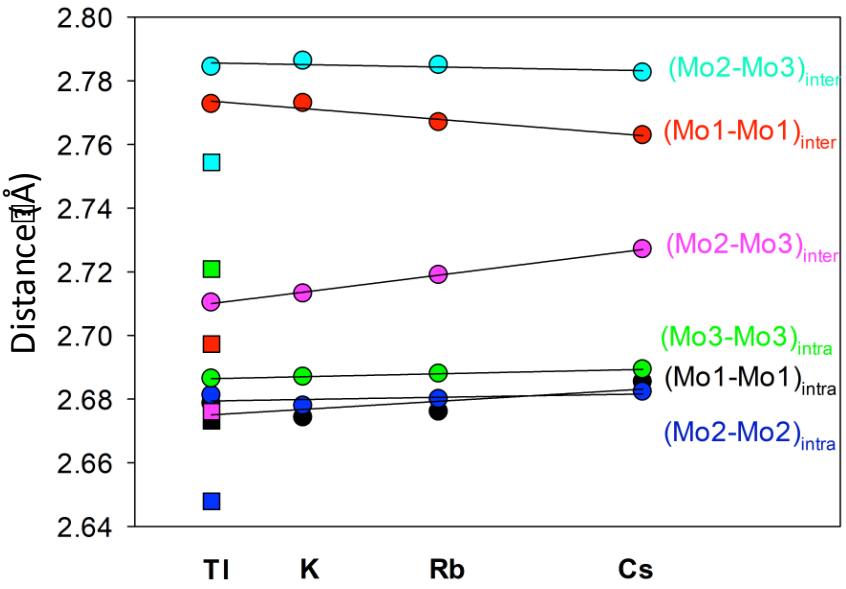

Figure 6

Journal Pre-proof

Journal Pre-proof

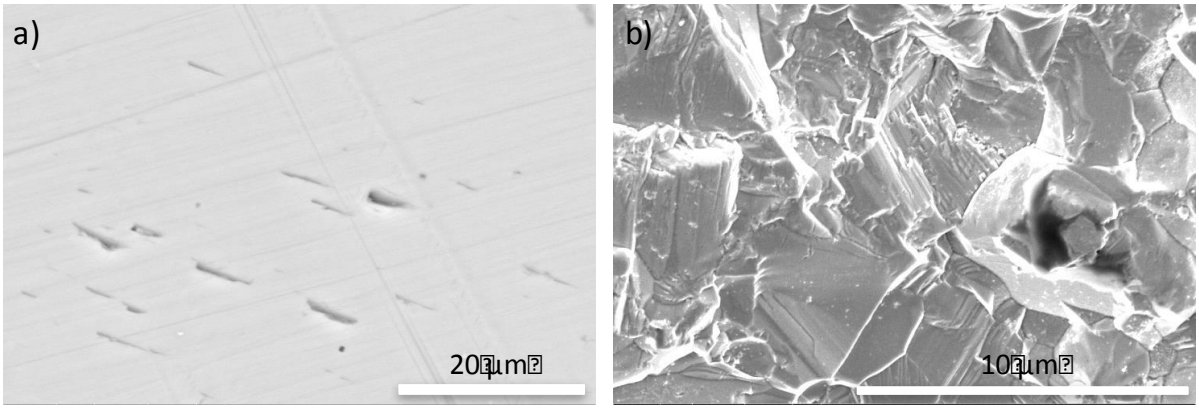

Figure 7

Journal Pre-proof

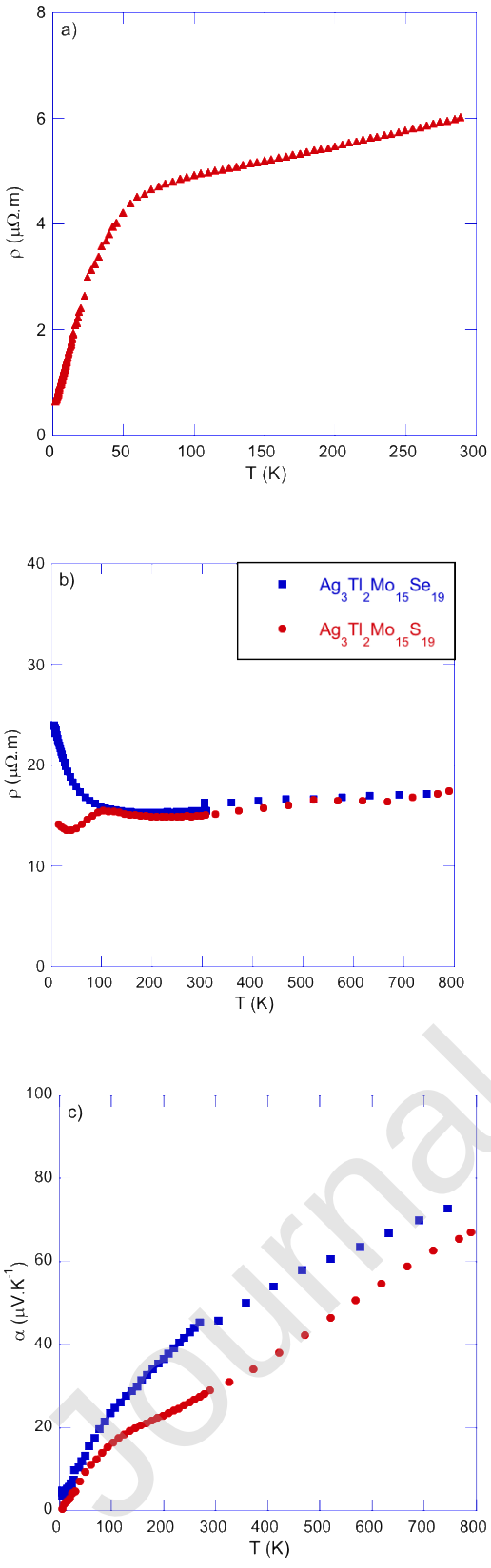

Figure 8

Journal Pre-proof

Journal Pre-proof

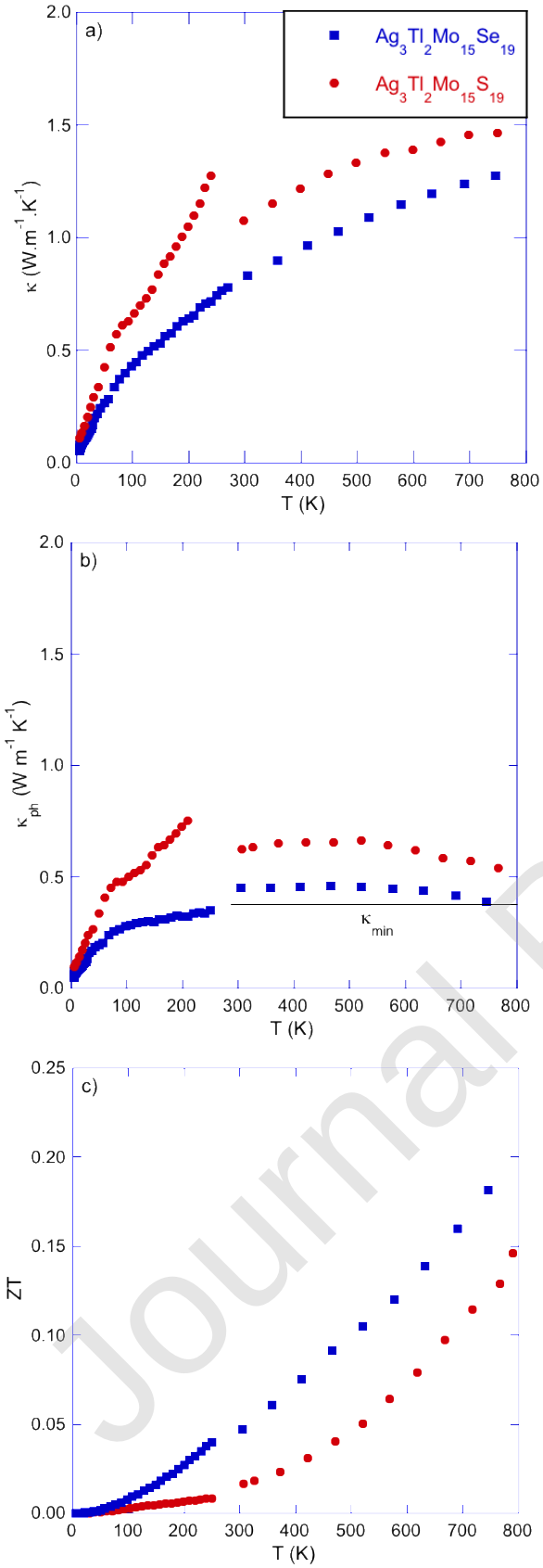

Figure 9